Determination of the surface deformation during the eruption of the Sakurajima volcano in February, 2016

Gergely LÁSZLÓ*, Lóránt FÖLDVÁRY*,**
* Óbuda University, Alba Regia Technical Faculty, Institute of Geoinformatics, Székesfehérvár, HUNGARY
** Hungarian Academy of Science, Research Centre for Astronomy and Earth Science, Geodetic and Geophysical Institute, Sopron, HUNGARY
laszlo.gergely@amk.uni-obuda.hu, foldvary.lorant@amk.uni-obuda.hu

***Abstract*—The present study provides an estimate of the vertical movements due to the most recent eruption of the Sakurajima volcano. The motion has been derived by using the InSAR technology; the paper gives an overview of the used data and applied methodology in details aiming to present sufficient information for providing a base for the reproducibility of the results. The observed vertical displacements are found to be reliable consequences of the eruption.**

I. INTRODUCTION

In April 03, 2014 a new era has begun in space-borne geodesy and remote sensing, with the launch of the Sentinel-1A satellite [1] in a joint Copernicus program of European Space Agency (ESA) and European Union (EU). The initial mission plans have contained three Sentinel series (1-3), with three satellite each (A, B, C), but after the first launch, a new satellite (Sentinel-1D) and three more series (4-6) has been added to the mission, which are scheduled to be launch after 2020 [2].

In this paper data produced by Sentinel-1A has been used. The main technical parameters are listed in Table 1 based on [1].

Apogee	693 km
Orbit regime	SSO (Sun-synchronous Orbit)
Inclination	98.18°
Period	98.6 minutes (175 orbit/cycle)
Repeat cycle	12 days
Mission duration	7 years, consumables for 12 years
Mission objectives	atmosphere-, marine- and land-monitoring, climate change, emergency management and security.

Table 1. Sentinel-1A data sheet [1]

Using the state-of-the-art vertical monitoring method, the Synthetic Aperture Radar Interferometry (InSAR) technology [3], a wide range of applications ranging from monitoring vertical displacement of discrete points, through monitoring movements of buildings, to observation of crustal movements on continental scale becomes feasible [4]. The SAR technology is an active remote sensing method [5], and as such, it is independent from the daytime cycle. The satellite radar interferometry is based on comparing one or more radar image. Using the phase values of the images phase differences can be derived, which are then interfered at the steady (i.e. being in no motion) areas. Based on the interferences, an interferogram can be deduced to estimate the amount of vertical movement at the area of interest [6].

II. CASE STUDY: SAKURAJIMA

The subject of this study is the determination of vertical displacements of the surface around the Sakurajima volcano before and after its eruption on 2016-02-05 [7], c.f. Figure 1. The volcano is located on the 3rd largest island of Japan, Kyushu (Figure 2), and is one of the most active volcanoes in Japan, performing several lava eruptions each year. The Sakurajima is a post-caldera volcano belonging to the Aira caldera in the northern half of Kagoshima Bay.The 17 x 23 km caldera has been formed about 22,000 years ago, which has been joined to the Osumi Peninsula during the major explosive and effusive eruption of 1914 [8].

Figure 1. Eruption of the Sakurajima

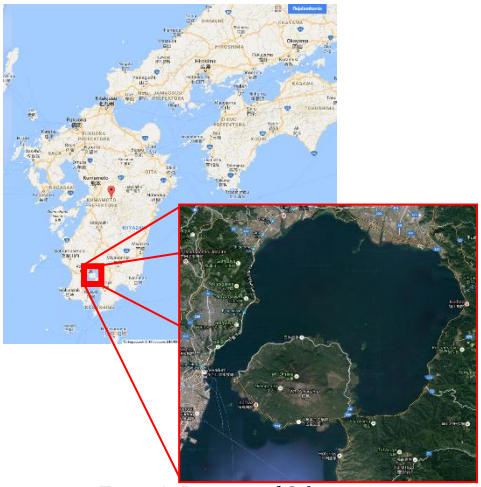

Figure 2. Location of Sakurajima

III. DATA PROCESSING

The data processing has been carried out by using an open-source software provided by the ESA, jointly developed by Brockmann Consult, Array Systems Computing and C-S for processing images of orbiting Sentinel satellites [9]. In this case data from the Sentinel-1A has been used, and most of the processing steps has been carried out with the Sentinel-1 Toolbox of the Sentinel Application Platform (SNAP) [9].

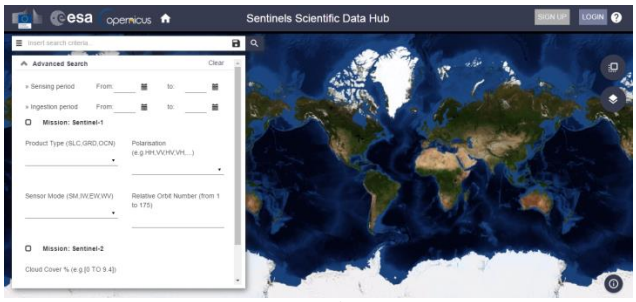

Figure 3. Scientific data hub

Two kind of data is available at the Sentinel Scientific Data Hub site (c.f. Figure 3): the SLC and the GRD. The SLC contains phase and amplitude values, while the GRD contains amplitude only. The present task has been done by using the SLC data as for the InSAR technique phases are the key information.

During the selection of SLC data, it is important to choose files 12 days apart from each other, otherwise the processing will not be possible [10]. The reason of this limitation is that the overlap between the images is only in every 175th full orbit complete [3]. As the most reliable information on vertical deformation can be derived from the vertical-vertical (abbr. VV) polarization [10], it has been set for the download. The time interval has been set between November 2015 and March 2016, and the area has been defined by a user-defined rectangular window. The search criteria are summarized in Table 2, and it has resulted in 7 images. Among them, 6 have been used, at the epochs summarized in Table 3.

Sensing period:	2015/11/01-2016/03/31
Satellite Platform:	S1A_*
Product Type:	SLC
Polarization:	VV
Relative Orbit Number:	163

Table 2. Search parameters

The most of the processing has been performed with the Sentinel-1 Toolbox of the SNAP software, apart from the determination of the vertical deformation map from the interferogram, which can be performed in an independent step with the use of the Statistical-Cost, Network-Flow Algorithm for Phase Unwrapping (SNAPHU) program. The major steps of the processing are as follows:

1. S1 TOPS Coregistration
2. Interferogram formation
3. S1 Tops Deburst
4. Topographic phase removal
5. Goldstein Phase Filtering
6. Phase Unwrapping
    a. Snaphu export
    b. Unwrapping
    c. Snaphu import
7. Phase to Displacement
8. Update Geo Reference
9. Ellipsoid Correction

During the *S1 TOPS Coregistration* step the master and slave images has been set. Every image (ref frame on Figure 4) contains three subsequent *Sub-swath*s (middle white frame on Figure 4), thus another selection has been made to choose that which part is the area should be processed. If necessary, the location can further be narrowed by using the tool *Bursts* (small white frames on Figure 4).

Date	Image filename
2015-11-28	S1A_IW_SLC__1SSV_20151128T211657_20151128T211724_008810_00C921_4D03
2015-12-22	S1A_IW_SLC__1SSV_20151222T211656_20151222T211723_009160_00D2EC_39F8
2016-01-15	S1A_IW_SLC__1SSV_20160115T211655_20160115T211722_009510_00DCEC_EE4A
2016-02-08	S1A_IW_SLC__1SSV_20160208T211654_20160208T211721_009860_00E70E_94CB
2016-03-03	S1A_IW_SLC__1SSV_20160303T211654_20160303T211721_010210_00F131_DF13
2016-03-27	S1A_IW_SLC__1SSV_20160327T211655_20160327T211722_010560_00FB2D_9908

Table 3. Images used during processing

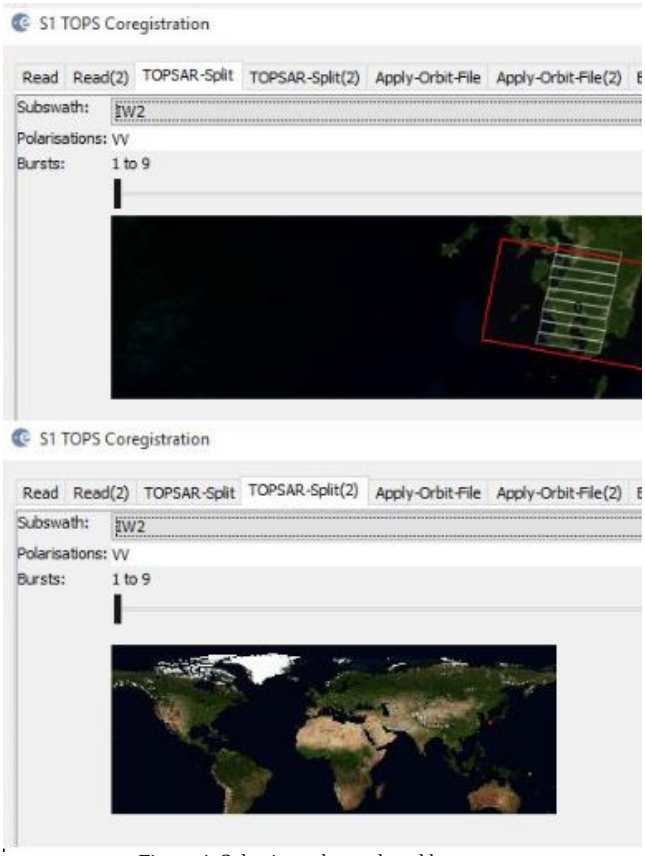

Figure 4. Selecting sub-swath and bursts

The selection shown on Figure 4 for the day 2015-12-22 provides the actual raw image shown on Figure 5, presenting the 9 bursts with interruptions (horizontal black lines) of the phase data (grey colors).

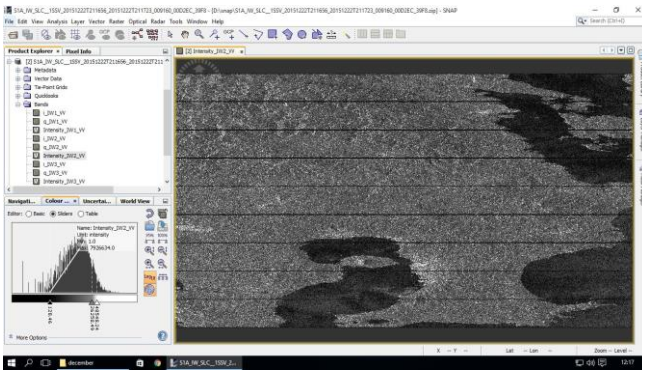
Figure 5. raw image on the day 2015-12-22

At the *Apply-Orbit_File* option *Sentinel Precise* has been set. The last setting here for the Elevation Correction is *Back-Geocoding*, where *SRTM 3Sec* has been chosen.

During the next step, the Interferogram formation, the following corrections are applied [11]:

- $\Delta\phi_{flat}$: phase correction for the Earth curvature (often named as *flat Earth phase*),
- $\Delta\phi_{elevation}$: phase correction due to topography,
- $\Delta\phi_{displacement}$: surface deformation correction,
- $\Delta\phi_{atmosphere}$ phase correction accounting for atmospheric differences,
- $\Delta\phi_{noise}$: phase noise correction generated by temporal change of the scatterers, varying look angle, and volume scattering.

The corrections are simply summed to a correction term, $\Delta\varphi$

$$\Delta\varphi = \Delta\varphi_{flat} + \ +\Delta\varphi_{displaceent} + \Delta\varphi_{atmosphere} + \Delta\varphi_{noise}$$

where:

$$\Delta\varphi_{flat} = -\frac{4\pi}{\lambda}\frac{B_n s}{R\tan\theta}$$

$$\Delta\varphi_{elevation} = -\frac{\Delta q}{\sin\theta}\cdot\frac{B_n}{R_0}\cdot\frac{4\pi}{\lambda}$$

$$\Delta\varphi_{displaceent} = +\frac{4\pi}{\lambda}d$$

In these equations B_n is the normal baseline, R_0 is the radar-target distance Δq is altitude difference, s is slant range displacement and θ is the radiation incidence angle with respect to the reference. (For the geometrical representation of some of these quantities, see Figure 6.)

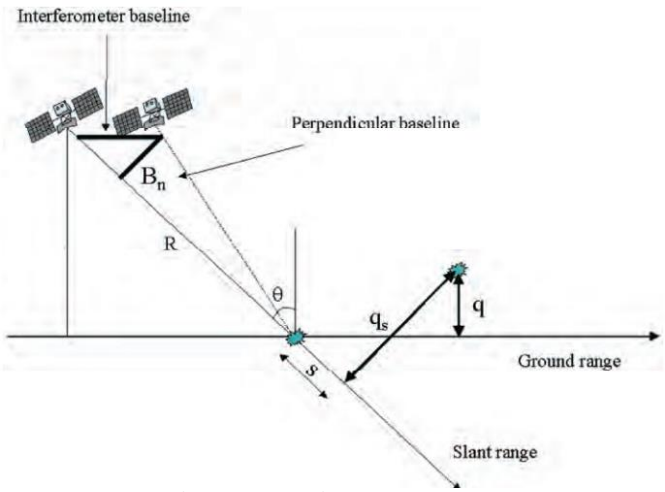

Figure 6. Sketch of the geometry of observing with a SAR satellite for the use of the InSAR technology. [12]

During *S1 Tops Deburst* step, the neighboring stripes are merged into one image, diminishing the bursts appearing on Figure 7.

Topographic phase removal is the subsequent step, which is based on a reference DEM (it can be defined arbitrarily, default setting is SRTM). Based on the DEM and the position of the satellite, the phases are simulated and considered to be a reference phase, which is therefore eliminated (c.f. Figure 7). The colors on Figure 7 are related to different values of phase ranging from 0 (red) to 2π (blue).

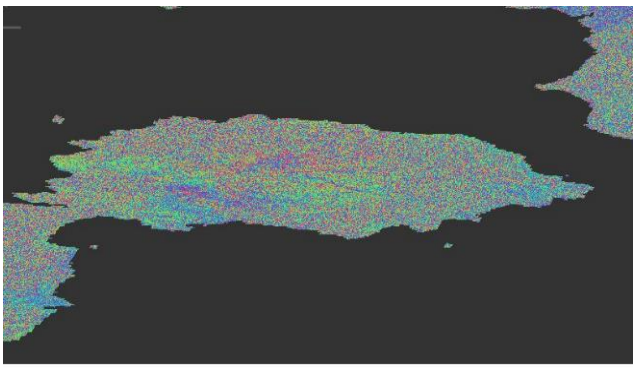

Figure 7. Phases after topographic phase removal (red=0 blue=2π).

The dotty characteristics of Figure 7 are a consequence of loss of coherence. The loss of coherence occurs due to temporal and geometric decorrelations, volume scattering and processing errors. This noisy feature can be reduced by applying *Goldstein Phase Filtering*, resulting on a much smooth image, c.f. Figure 8.

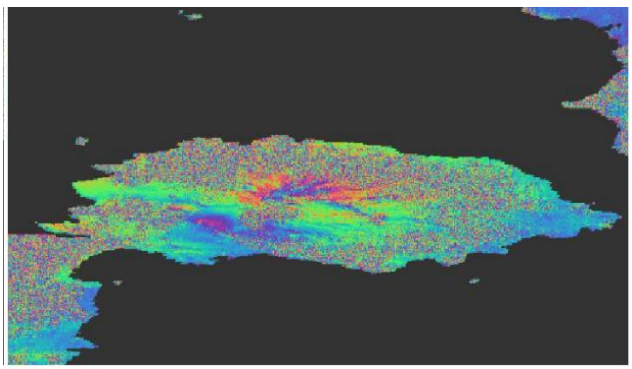

Figure 8. Phases after the Goldstein filter has been applied (red=0 blue=2π).

The interferometric phase on Figure 8 is ambiguous, since it is only known in the interval of 0 to 2π. In order to convert the interferometric phase to the topographic height, the so-called *Phase Unwrapping* should be performed, i.e. the phases must be extracted („unwrapped"). For this step, the images can be processed in a separated software (SNAPHU) and for this, exporting then importing of the date is necessary.

Phase to Displacement is a function to convert phases in radian to vertical displacement in meters.

In order to transform the results into geographical coordinate system, two other function, the *Update Geo Reference* and the *Ellipsoid Correction* should be used. The final results of the vertical deformation are presented on Figure 9 and Figure 10. On Figure 9 the surface deformation between 15 January and 8 February is shown, while Figure 10 display the vertical change between 8 February and 3 March.

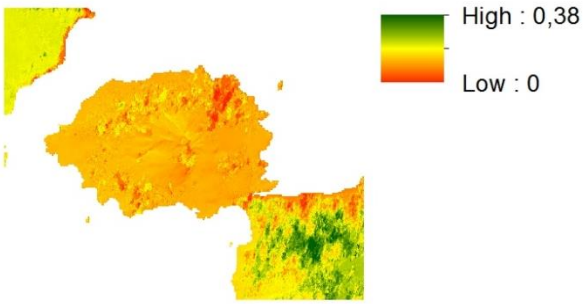

Figure 9. Surface deformation between 15 January, 2016 and 8 February, 2016.

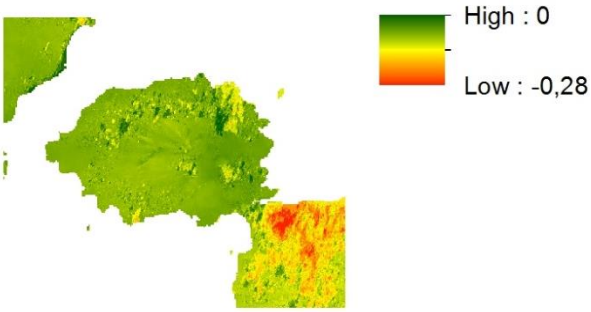

Figure 10. Surface deformation between 8 February, 2016 and 3 March, 2016.

IV. RESULTS

As the eruption has been occurred in 5 February, 2016, Figures 9 and 10 are reliable snapshots of the surface deformations before (Figure 9) and after (Figure 10) of the eruption. In fact, there is a 3-day time lag between the eruption (5 February) and the scan of the middle image (8 February), which leaves sufficient time for near real time relaxations, thus present comparison can be interpreted as long-term relaxations of the ground.

A classical method for monitoring crustal deformation of a volcano in order to predict eruptions is the observation of the slope angle or tilt of the ground in the vicinity of the volcano [13]. Obviously, when the magma pushes the ground upward, the slope of the nearby areas tilts away from the center of uplift. This happens before the eruption. Similarly, when the ground subsides due to

depressurization of the magma chamber, the slope of neighboring areas tilts toward the center of subsidence. The leave of high pressure gases (and some magma) from the magma body definitely results in depressurization of the region. Thus uplift before the eruption and subsidence after the eruption may be expected.

According to Figures 9 and 10, before the eruption the uplift of the curst has reached an approximate average value of *+15 cm*, and the subsidence of the region after the eruption reached the average value of *-7 cm*. This 22 cm change in surface elevation is reliable according to the overall analysis of [14], which has found eruption related surface deformation to be in similar range.

Tilt measurements and increasing seismic activity provides a good base for prediction, but these techniques may provide no information on the eruption-related surface deformations. Measurement of surface deformation of this amount with repeated leveling measurements may be challenging, since the magma chamber is extended far beyond the area of the volcano, so no fix benchmarks in the nearby are available. For the purpose, the InSAR technique was found to be a competent tool.

ACKNOWLEDGMENT

The authors would like to express their gratitude to prof. László Bányai for the valuable support and consultations, and also for providing an access to the processing facility at the Geodetic and Geophysic Institute of MTA CSFK.

REFERENCES

[1] Sentinel-1: ESA's Radar Observatory Mission for Copernicus Operational Services, *S1 Data Sheet*, homepage: http://esamultimedia.esa.int/docs/S1-Data_Sheet.pdf, retrieved 2016-10-18.

[2] ESA, Copernicus: Observing the Earth, homepage: http://www.esa.int/Our_Activities/Observing_the_Earth/Copernicus/Overview3, retrieved 2016-10-18.

[3] L. Bányai, E. Szűcs, J. Kalmár, I. Eperné Pápai, D. Bán, "Az InSAR technológia alapjai és a reflektáló felületek jellemzői", *Geomatikai Közlemények*, vol. XVII, pp. 59-68, 2014.

[4] M. Simons and P. A. Rosen, "Interferometric Synthetic Aperture Radar Geodesy", *Treatise on Geophysics*, vol. 3, pp. 391-446, 2007.

[5] A. Moreira, P. Prats-Iraola, M. Younis, G. Krieger, I. Hajnsek, K.P. Papathanassiou, "A tutorial on synthetic aperture radar". IEEE Geoscience and Remote Sensing Magazine. vol. 1, pp. 6-43, 2013. doi:10.1109/MGRS.2013.2248301

[6] R. F. Hanssen, "Satellite radar interferometry for deformation monitoring: a priori assessment of feasibility and accuracy", International Journal of Applied Earth Observation and Geoinformation, vol. 6, pp. 253–260, 2005.

[7] Sakurajima volcano in Japan erupts: Lava rolls down mountain's slope and smoke billows into sky after eruption in southern Japan, *The Guardian*, Associated Press, 5 February 2016, link: https://www.theguardian.com/world/2016/feb/05/sakurajima-volcano-japan-erupts, retrieved 2016-10-18.

[8] Sakurajima at the Global Volcanism Program, *Smithsonian Institution National Museum of Natural History*, link: http://volcano.si.edu/volcano.cfm?vn=282080, retrieved in 2016-10-18.

[9] Sentinel-1 Toolbox of the Sentinel Application Platform (SNAP), available at the Science Toolbow Exploitation Platform (STEP); link: http://step.esa.int/main/toolboxes/snap/, retrieved 2016-10-18.

[10] L. Bányai: private discussion, 2016.

[11] L. Veci, "Sentinel-1 Stripmap Interferometry: Sentiel-1 Toolbox Interferometry Tutorial", Array Systems Computing Inc., pp. 41, 2015.

[12] K Fletcher (ed.), "InSAR Principles: Guidelines for SAR Interferometry Processing and Interpretation (TM-19, February 2007)", ESA Publications, ESTEC, Postbus 299, 2200 AG Noordwijk, The Netherlands, pp. 48, ISBN: 92-9092-233-8, ISSN: 1013-7076, 2007.

[13] M. Battaglia, P. F. Cervelli and J. R. Murray, "Modeling Crustal Deformation near Active Faults and Volcanic Centers — A Catalog of Deformation Models", Techniques and Methods 13–B1, Chapter 1 of Section B: Modeling of Volcanic Processes, Book 13: Volcanic Monitoring, U.S. Department of the Interior, U.S. Geological Survey, Reston, Virginia, pp. 108, 2013.

[14] J. Biggs, E. Robertson and K. Cashman, "The lateral extent of volcanic interactions during unrest and eruption", Nature Geoscience, vol. 9, pp. 308–311, doi:10.1038/ngeo2658, 2016.